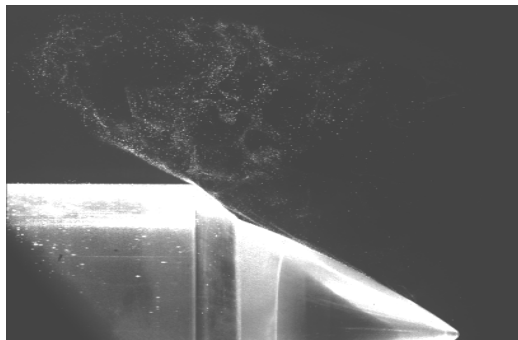




Master's Degree Thesis

ISRN: BTH-AMT-EX--2008/D-10--SE

# Setup of Particle Image Velocimetry (PIV) in Hypersonic Flows



**Moazzam Anwar**

Department of Mechanical Engineering  
Blekinge Institute of Technology  
Karlskrona, Sweden

2008

---

Supervisors: Ansel Berghuvud, Ph.D Mech Eng, BTH  
Prof. Dr.-Ing. Rolf Radespiel, Technical University Braunschweig, Germany



# Setup of Particle Image Velocimetry (PIV) in Hypersonic Flows

**Moazzam Anwar**

**Department of Mechanical Engineering**

**Blekinge Institute of Technology**

**Karlskrona, Sweden**

**2008**

Thesis submitted for completion of Master of Science in Mechanical Engineering with emphasis on Structural Mechanics at the Department of Mechanical Engineering, Blekinge Institute of Technology, Karlskrona, Sweden.

## **Abstract:**

The accuracy of numerical methods in calculating the flow of backward facing steps in turbulent hypersonic flows is limited due to a lack of flow measurements. Such measurements are necessary to validate numerical techniques and turbulent models. The lack of measurements concerns especially quantitative data on the dynamics of large turbulent structures. One approach to solve this problem is to measure the global velocity field. Therefore the Particle Image Velocimetry (PIV) has to be arranged for the use in high speed flows. In this project PIV setup was installed for the use in hypersonic Ludwig tube Braunschweig (HLB). After the setup of PIV system, a generic hyperboloid-flare configuration was examined. The influence of shocks on particle concentration can be identified in these measurements. On this model previous infrared thermography measurements and numerical calculations are available, therefore a comparison was made.

## **Keywords:**

Hypersonic Ludwig tube Braunschweig (HLB), Particle Image Velocimetry(PIV), Generic Hyperboloid flare configuration.

# Foreword

*“When Almighty created the openings of atmosphere, expanse of firmament and strata of winds, He flowed into it water whose waves were stormy and whose surges leapt one over the other. He loaded it on dashing wind and breaking typhoons, ordered them to shed it back (as rain), gave the wind control over the vigour of the rain, and acquainted it with its limitations. The wind blew under it while water flowed furiously over it.”*

(Nahjul Balagha: Sermon 1)

Human beings natural instincts provoke them to have knowledge about nature and make best use of it for their survival. The history of fluid mechanics can be traced back to the days of ancient Greece, when Archimedes made a beginning on the fluid statics. Later in medieval times Muslim Physicists, Abu Rayhan al Biruni and Al-Khazini developed fluid dynamics. However, fluid mechanics, especially fluid dynamics, is an active field of research with many unsolved or partly solved problems. Fluid mechanics can be mathematically complex. Sometimes it can best be solved by numerical methods, typically using computers. A modern discipline, called *Computational Fluid Dynamics* (CFD), is devoted to this approach to solving fluid mechanics problems. Also taking advantage of the highly visual nature of fluid flow is Particle Image Velocimetry(PIV), an experimental method for visualizing and analyzing fluid flow.

# Acknowledgements

This work was carried out at Institute of Fluid mechanics, Technical University Braunschweig, Germany, under the supervision of Prof. Dr.-Ing. Rolf Radespiel, Dr.rer.nat.habil. Christian J. Kähler, Dipl.-Ing. Dirk Heitmann and Dipl.-Ing. Peter Scholz.

The work is a part of research projects being carried out at Institute for Fluid mechanics, TU Braunschweig, Germany, under the workgroup of Flow Control and Measuring Techniques. I studied there as an Erasmus exchange student. The work started in Feb, 2008.

I extend my greatest gratitude's to the whole group for their guidance and professional engagement throughout the work. My special thanks to Dirk Heitmann for his time based guidance from the start of work till the completion of report. Also, thanks to my supervisor Dr. Ansel Berghuvud at home university (Blekinge Institute of Technology, Karlskrona, Sweden) for his valuable suggestions and support.

In the end thanks to my beloved family whose moral support encouraged me to anticipate actively in the work.

Karlskrona, October 2008,

*Moazzam Anwar*

# Contents

<b>1 Notation</b>	<b>6</b>
<b>2 Introduction</b>	<b>8</b>
2.1 Aim and Scope of the work.	10
<b>3 Particle selection</b>	<b>12</b>
3.1 scattering characteristics of particles.	12
3.2 Tracking characteristics of particles.	14
3.2.1 Equation of Motion.	14
3.3 Health and Hazardous Impacts of Seeding Particles.	18
3.4 Cost Concerns.	21
3.5 Considerations about CO <sub>2</sub>	21
3.6 TiO <sub>2</sub> as Seed Material.	23
<b>4 Seeding generator and seeding system.</b>	<b>26</b>
4.1 Experimentation with seeding system.	28
4.1.1 Particles Measurements.	28
<b>5 Experimental work.</b>	<b>31</b>
5.1 Facility Description.	31
5.1.1. Working Principle.	31
5.2 Hyperboloid Model.	32
5.3 Illumination and Photo acquisition system.	33
5.4. Experimentation.	34
5.5. Data Processing.	35
5.6 Comparison of Experimental work with Numerical Work	38
5.7 Image Position error.	42
<b>6 Conclusions.</b>	<b>46</b>
<b>7 Recommendations for Future Research.</b>	<b>48</b>
<b>8 References.</b>	<b>49</b>

## **Appendices**

A Bolt Selection Formula.	51
B Particle measurements.	52

# 1 Notation

$A$	Area of the surface (top lid)
$A_{bolt}$	Area of the bolt
$C_s$	Scattering cross section
$d_p$	Diameter of the particle
$d_p(t)$	Particle diameter at time $t$
$d_p(i)$	Particle initial diameter
$H_v$	Latent heat of sublimation
$I_o$	Laser intensity incident on particle
$K_a$	Thermal conductivity
$M$	Scale factor in mm/pix
$Nu$	Nusselt no
$m$	Refractive index
$n_{bolt}$	no of bolts.
$\Delta P$	Total pressure on the surface (top lid)
$P_s$	Total scattered power
$S$	Safety factor
$\sigma_{max}$	Tensile strength of bolt,
$T_\infty$	Gas temprature
$T$	Particle temprature
$\Delta t$	Time delay between the two laser pulses
$U_p$	Particle velocity
$U_f$	Fluid velocity
$U_g$	Gravitational induced velocity

$U_s$	Particle step response velocity
$U_p(t)$	Particle instantaneous velocity
$U(t)$	Actual particle velocity normal to the shock
$U_1$	Particle velocity upstream of shock
$U_2$	Flow velocity downstream of shock
$V$	Particle ensemble velocity
$V(t)$	Instantaneous particle velocity
$\Delta V_p$	Particle velocity error
$\nabla \vec{V}_p$	Velocity gradient
$\Delta x$	Distance travelled by the particle in two frames in pixels
$\lambda$	Laser wavelength
$\tau_s$	Particle relaxation time
$\rho_p$	Particle density
$\mu$	Dynamic viscosity
$\rho_f$	Fluid density
$\xi$	Besset integral term
$\nabla \vec{\xi}$	Optical displacement gradient

## 2 Introduction

The development of Particle Image Velocimetry (PIV) is attributed to the non-intrusive methods for the velocity measurements in different flow regimes. The salient advantage of this technique is to investigate high speed flows with shocks or in boundary layers close to the wall, where the flow may be disturbed by the presence of probes.

The PIV technique uses the tracer particles which are injected into the flow. The measured velocity of these tracer particles reveals the velocity of the fluid elements

The experimental set-up of a PIV system consists of several sub systems. Above all a seeding system is required to inject the proper seeding particles into the flow. These particles are then illuminated by the laser sheet in the plane of the flow at least twice within short time interval. The light scattered by the particles has to be recorded either on a single frame or on a sequence of frames. The displacement of the particle images between the light pulses has to be determined through evaluation of the PIV recordings. The formula for determining the velocities of the particle is given below in equation (2.1).

$$V = \frac{M \cdot \Delta x}{\Delta t} = \frac{M}{\Delta t} \int_{\Delta t} V(t) dt \quad (2.1)$$

Where,

$V$  = Particle ensemble velocity,

$\Delta x$  = Distance travelled by the particle in two frames in pixels.

$M$  = Scale factor in mm/pix.

$\Delta t$  = Time delay between the two laser pulses.

In order to be able to handle the great amount of data which can be collected employing PIV technique, sophisticated post-processing is required.

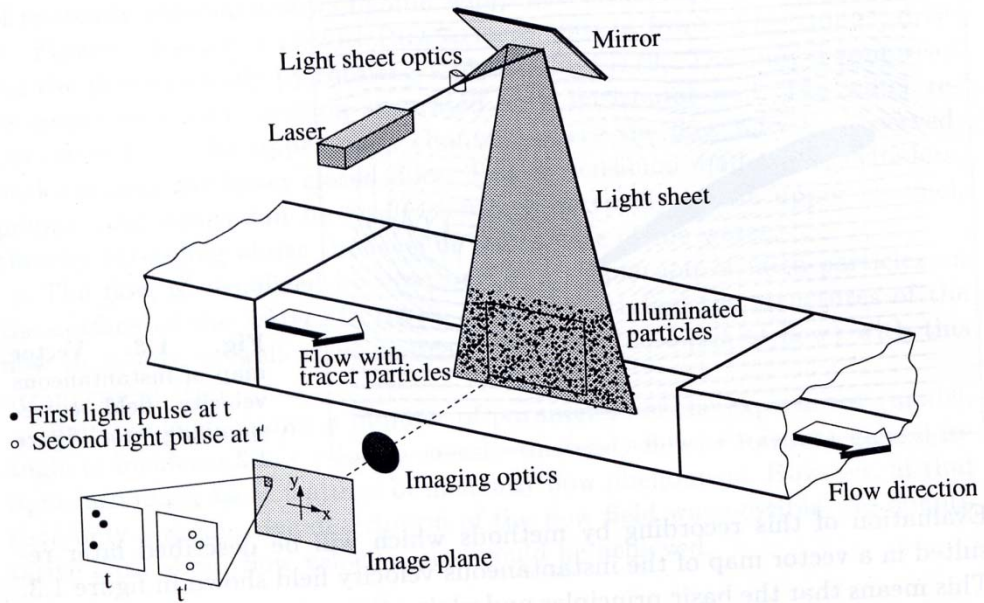


*Figure 2.1. Experimental arrangement for particle image velocimetry in a wind tunnel [1]*

Figure 2.1 explains the typical setup for the PIV recording in a wind tunnel. Small tracer particles are added to the flow. A plane (light sheet) within the flow is illuminated twice by means of a laser (the time delay between pulses depending on the mean flow velocity and the magnification at imaging).

It is assumed that the tracer particles move with local flow velocity between the two illuminations. The light scattered by the tracer particles is recorded via a high quality CCD camera. The cross correlation on photographic PIV is done by means of a software to unfold the information. The sequential representation of the work is shown in figure (2.2).

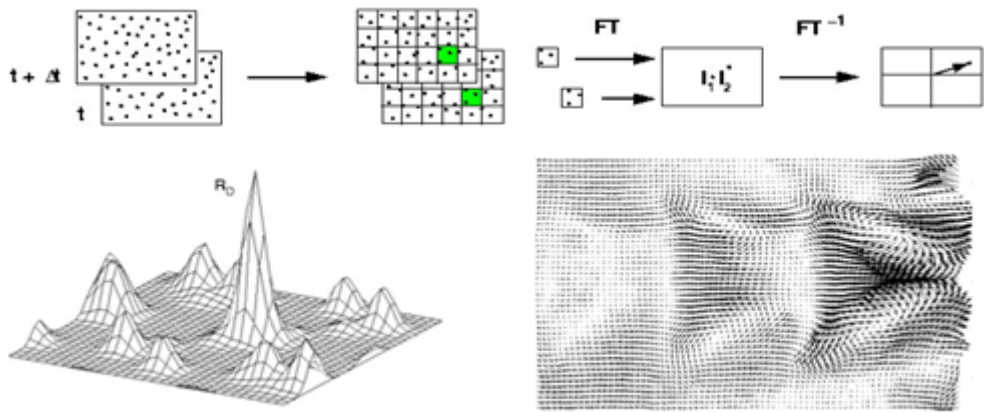


Figure 2.2. Analysis of double frame/single exposure recordings: the digital cross correlation method [2].

PIV is a technique which allows one to record images of large parts of flow fields in a variety of applications in gaseous and liquid media and to extract the velocity information out of these images. With PIV spatial resolution is large.

## 2.1 Aim and Scope of the Work

The objective of the current work is to install a PIV system in Hypersonic Ludweig tube Braunschweig (HLB). The purpose of the setup is to analyze the flow around a generic hyperboloid - flare configuration and then comparison of the PIV results with the already available infrared thermography measurements and numerical calculations.

A comprehensive summary of the works is given below for the attainment of the above stated goal.

The very first task is the selection of proper seeding material. The selection of the seeding material is very crucial because properly selected material follows the flow faithfully as well as reflects the enough light for the image processing. Also the health and hazardous impacts as well as the cost concerns are major issues to be addressed in particle selection criteria.

The second task is the design of seeding generator for the homogenous distribution of particles in the wind tunnel. The safe design of the seeding

generator requires proper selection of the material and fasteners to withstand the intended pressure. The air purging pipe should produce proper swirl for the outburst of the particles from the seeding generator. Burst test is carried out on seeding generator to ensure its safe usage.

Also the delivery of the particles from the seeding generator at different pressure ratios between seeding generator and ambient (within pressure vessel) and seeding generator filling level are measured to ensure that there are enough particles during the experiments.

Then comes the installation of lasers, camera and the model. After the proper installation (described in the relevant sections) of the lasers, camera and model, the synchronization problems of these equipments are resolved. It is assured that the camera captures the picture of the flow within the tunnel run time.

After the completion of the above stated works, experiments are carried out showing particle movements.

Cross- correlation is performed on the images to get the information of the velocities of the particles. The results then show shock waves resulting from the interaction of the fluid with the model.

A comparison is made between the results from PIV and numerical simulations (computed with TAU code) [11].

Particle position error is calculated. This position error contributes to the direct velocity error (bias error).

## 3 Particle Selection

The very fundamental step in the PIV is the selection of a proper particle material and size. There are some considerations to be kept in mind to achieve the optimal results. Among those are, the size of the particles should be large enough to scatter sufficient light for image acquisition, but should also be small enough to faithfully follow the flow. Lastly, the impact of the seeding particles to our equipment as well as to our health must be considered.

### 3.1 Scattering characteristics of Particles

The image intensity acquired from the particles and therefore the contrast of the PIV recordings is directly proportional to the scattered light power, it is often more effective and economical to increase the image intensity by properly choosing the scattering particles than by increasing the laser power. In our case particles of small sizes (50nm to 10 $\mu$ m) are required due to low density of the flow. It is because small particles will follow the flow faithfully.

The light scattering capability of particle is described as the scattering cross section  $C_s$ , defined as the ratio of the total scattered power  $P_s$  to the laser intensity  $I_o$  incident on the particle;

$$C_s = \frac{P_s}{I_o} \tag{3.1}$$

Table 3.1. Scattering cross sections as a function of particle size [3].

Diameter $d_p$	Scattering cross section $C_s$	
<b>Molecule</b>		$\cong 10^{-33} m^2$
<b>1 <math>\mu m</math></b>	$C_s \cong \left( \frac{d_p}{\lambda} \right)^4$	$\cong 10^{-12} m^2$
<b>10 <math>\mu m</math></b>	$C_s \cong \left( \frac{d_p}{\lambda} \right)^2$	$\cong 10^{-9} m^2$

The variation of the scattering cross section as a function of the ratio of the particle diameter ( $d_p$ ) to the laser wavelength ( $\lambda$ ) for the spherical particles with refractive index  $m=1.6$  is shown in the figure 3.1 below.



Figure 3.1: The scattering cross section as a function of particle size (refractive index  $m = 1.6$ ) [3]

It is very obvious from the Table 3.1 and Figure 3.1 that the scattering cross section increases with the increase in particle size.

In PIV experiments light scattered at  $90^\circ$  from the incident light sheet is observed. Therefore, the angular distribution of the scattered light as well as the scattering cross section is important. The angular distribution of scattered light in the vicinity of  $90^\circ$  is complex, with several nodes whose exact positions are strongly size dependent [4]. The influence of these fluctuations can be reduced by spatial averaging over a finite aperture of the collecting optics. The ratio  $I_{90}/I_{s0}$  decrease with the increase in size parameter value  $d_p/\lambda$ , with the values roughly in the range of  $10^{-1} - 10^{-3}$  for scattering particles useful in PIV.

## 3.2 Tracking Characteristics of Particles

### 3.2.1 Equation of Motion

Beset [5] gave the equation for unsteady motion of a suspended sphere. This equation relates the instantaneous relative velocity  $V = U_p - U_f$  between the particle and the fluid to the instantaneous velocities  $U_p$  and  $U_f$  of the particle and fluid respectively. These velocities are represented as in figure 3.2;

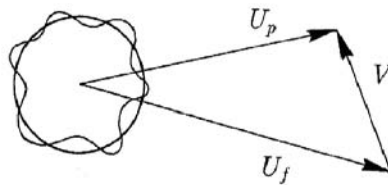


Figure 3.2.: Suspended particle's relative motion.

$$\frac{\pi d_p^3}{6} \rho_p \frac{dU_p}{dt} = -3\pi\mu d_p V + \frac{\pi d_p^3}{6} \rho_f \frac{dU_f}{dt} - \frac{3}{2} d_p^2 (\pi\mu\rho_f)^{1/2} \int_{t_0}^t \frac{dV}{d\xi} \frac{d\xi}{(t-\xi)^{1/2}} \quad (3.2)$$

where;

$d_p$  =particle diameter

$\rho_p$  =particle density

$\mu$  =Dynamic viscosity

$\rho_f$  =Fluid density

$\xi$  =Basset integral term

The acceleration force and the viscous resistance according to stroke's Law are given in the first two terms. The acceleration of the fluid leads to a pressure gradient in the vicinity of the particle and hence to an additional force given by the third term. The fourth term represents the resistance of an inviscid fluid to the acceleration of the sphere, as given by the potential theory. The final term is the 'Basset history integral' which defines the resistance caused by the unsteadiness of the flow field.

For PIV in gas flows, the focus of this research, the density ratio of the seed material is much greater than the density of the fluid, and the equation of motion for a particle shown in Equation (3.3) becomes dominated to the Stokes terms, resulting in the following expression:

$$\frac{dU}{dt} = -\frac{18\mu}{\rho_p d_p^2} (U_p - U_f) \quad (3.3)$$

This relationship compares favourably to the work published by Raffel, Willert and Kompenhans [6], who describes the primary source of error in tracer particle motion in steady flows as the influence of gravitational forces when the density of the fluid  $\rho$  and the tracer particles  $\rho_p$  are not the same.

The gravitationally induced velocity  $U_g$  from Stokes drag law is determined in order to introduce how the particles behave under accelerations. Stokes drag law assumptions are applicable when the particle is assumed spherical

and the particle's Reynolds number is small, which is applicable for tracer particles in gas flows [6, 7].

The gravitationally induced velocity is.

$$U_g = d_p^2 \frac{(\rho_p - \rho_f)}{18\mu} g \quad (3.4)$$

Raffel, et al[1] further relate the gravitational induced velocity equation above to derive an estimate for the velocity lag of a particle in a continuously accelerating fluid:

$$U_s = U_p - U = d_p^2 \frac{(\rho_p - \rho_f)}{18\mu} a \quad (3.5)$$

They further determined that the step response of the seed particle ( $U_p$ ) typically follows an exponential law if the density of the particle is much greater than the fluid density. This difference in density is a characteristic of using solid tracer particles in gaseous flows. This results in the development of a relationship for particle velocity  $U_p(t)$  by Melling [3] which is:

$$U_p(t) = U \left[ 1 - \exp\left(-\frac{t}{\tau_s}\right) \right] \quad (3.6)$$

The particle velocity response in the wake of a shock can be tracked by the work of Melling (1997) [3].

$$U_p(t) = \frac{U(t) - U_1}{U_2 - U_1} = e^{-t/\tau_s} \quad (3.7)$$

Where  $U(t)$  is the actual particle velocity normal to the shock at a given instant.  $U_1$  is its value upstream of the shock and  $U_2$  is the flow velocity downstream of the shock.

$\tau_s$  is the relaxation time and is given by the equation.

$$\tau_s = d_p^2 \frac{\rho_p}{18\mu} \quad (3.8)$$

Relaxation time is a convenient measure of the tendency of the particle to achieve equilibrium with the fluid. Thus it is one of the fundamental step in selecting the particle material and size.

Plots of relaxation time are depicted in the figure (3.5) below. It is very obvious that the particles with smaller diameter tend to achieve the equilibrium with the fluid velocity earlier than the larger particles.

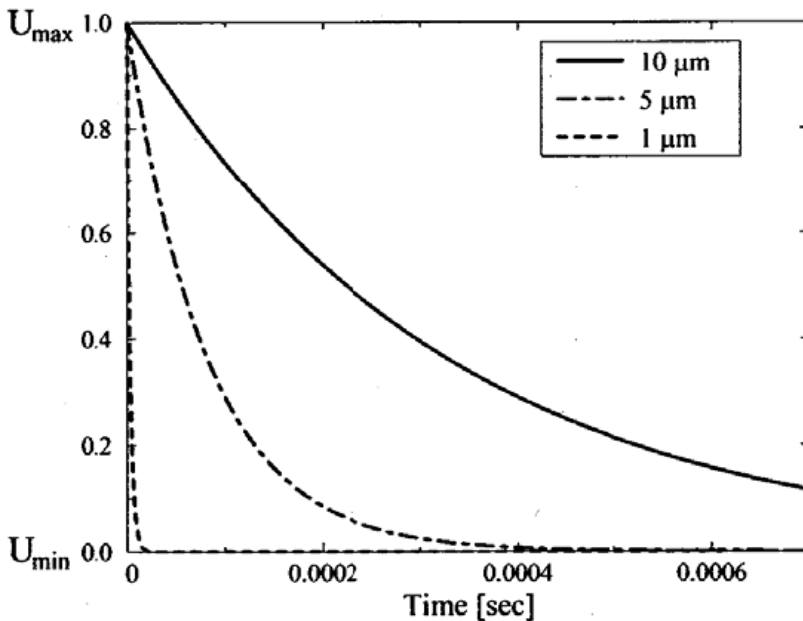


Figure 3.4.: A Typical Relaxation Time as a Function of Particle Size [1]

Some properties of the commonly used seeding particles in the gas flows are depicted in the table 3.2 below.

Table 3.2. Seeding particles in gas flows[3].

Material	$d_p$ ( $\mu\text{m}$ )	Laser	Pulse energy, pulse time	Light sheet		Reference
				$w$ (mm)	$t$ (mm)	
TiO <sub>2</sub> ( $m = 2.6$ , $\rho = 3500 \text{ kg m}^{-3}$ )	<1	Nd:YAG	10 mJ, 20 ns	15	0.3	Reuss <i>et al</i> (1989)
TiO <sub>2</sub> , ZrO <sub>2</sub>	0.7–1	Nd:YAG	110 mJ, 12 ns			Paone <i>et al</i> (1996)
Al <sub>2</sub> O <sub>3</sub> ( $m = 1.76$ , $\rho = 3970 \text{ kg m}^{-3}$ )	0.3	Nd:YAG	400 mJ		0.2	Muniz <i>et al</i> (1996)
	3	Nd:YAG	9 mJ, 6 ns			Anderson <i>et al</i> (1996)
	0.8	Ruby	20 ns	150	$\approx 1$	Krothapalli <i>et al</i> (1996)
Polycrystalline	30	Nd:YAG	135 mJ, 6 ns			Grant <i>et al</i> (1994)
Glass	30	Ruby	30 mJ, 30 ns			Schmidt and Löffler (1993)
Oil smoke	1	Ruby	5 J			Stewart <i>et al</i> (1996)
Corn oil	1–2	Nd:YAG	100 mJ			Jakobsen <i>et al</i> (1994)
Oil	1–2	Nd:YAG	120 mJ		0.4	Westerweel <i>et al</i> (1993)
Olive oil ( $m = 1.47$ , $\rho = 970 \text{ kg m}^{-3}$ )	1.06	Nd:YAG	70 mJ, 16 ns	200	0.5	Höcker and Kompenhans (1991)
						Fischer (1994)
						Raffel <i>et al</i> (1996)

### 3.3 Health and Hazardous Impacts of Seeding Particles

As the particles employed in PIV can pose serious damaging effects to the health of the people working with them, to the environment as well as to the equipment. Therefore special attention is needed to choose the right seeding material that is more users friendly. We list below some of the Health and Hazardous Impacts of the Seeding Particles, addressed in the conference on PIV, by R. D. Brown of the Kelsey-Seybold Clinic PA (7). Also the conclusion of IARC (International Agency for Research on Cancer) for Titanium Dioxide is incurred in the table (3.3) below. It suggested that Titanium Dioxide is Carcinogenic to humans (Group 2B) through inhalation not digestion. This classification is based upon animal inhalation studies. Epidemiology studies do not suggest an increased risk of cancer in humans from occupational exposure to titanium dioxide.

An approximation of physiological classification of toxicities is provided below in Table (3.3):

*Table 3.3. Physiological Classifications of Toxic Materials[8]*

<b>Class</b>	<b>Examples</b>
Irritant	Ammonia, Sulphur Dioxide
Asphyxiant	Nitrogen Dioxide, Carbon Monoxide and Dioxide
Anesthetic	Aliphatic Hydrocarbons, Ethyl Alcohol
Systemic Poison	Heavy Metals, Carbon Tetrachloride
Sensitizer	Isocyanates, Formaldehyde
Fibrotic Agent	Silica, Coal Dust
Mutagens and Carcinogens	Arsenic, Asbestos, Titanium Dioxide
Nuisance	Alumina, Kaolin, Magnesia

The American Conference of Governmental Industrial Hygienists (ACGIH) publishes a size distribution guide describing how respirable particulates may be, and is summarized in Table (3.4).

*Table 3.4. Respirable Particulate Size Distribution[8]*

<b>Particulate Size (<math>\mu\text{m}</math>)</b>	<b>% Respirable</b>
< 2	90
2.5	75
3.5	50
5.0	25
10	0

Particulate seeding materials also pose explosive hazards. A commonly referenced property that adequately describes the volatility is vapour pressure, and is often expressed as a material's lower explosive limit. The lower explosive limit is the minimum air concentration at which a homogeneous mixture can be burned when subjected to an ignition source

of adequate temperature and energy. A synopsis of the health and safety hazards for common seed materials is provided in Table 3.5.

*Table 3.5: Health and Hazard Properties of Seed Materials[8]*

<b>Name</b>	<b>Exposure Limit</b>	<b>Health Effects</b>	<b>LEL</b>
Aluminium Oxide	10 mg/m <sup>3</sup>	Nuisance, Carcinogen	N/A
Titanium Dioxide	10mg/m <sup>3</sup>	Carcinogen	N/A
Kaolin	10 mg/m <sup>3</sup>	Nuisance	
Silicon Carbide	10 mg/m <sup>3</sup>	Nuisance	
Polystyrene Latex	10 mg/m <sup>3</sup> 50 ppm	Nuisance, Carcinogen Anesthetic, Irritant	15 g/m <sup>3</sup> 1.1%
Vinyl Toluene	10 mg/m <sup>3</sup> 50 ppm	Nuisance Anesthetic, Irritant	0.1%
Propylene Glycol		Nuisance	2.6%
Kerosene	14 ppm	Irritant	0.9%
Ethyl Alcohol	1000 ppm	Anesthetic, Irritant	3.3%
Methyl Alcohol	200 ppm	Anesthetic, Irritant	6.7%

Comparatively CO<sub>2</sub> is less hazardous to work with, readily available and the health concerns are little as well. The significant hazard in the solid form will be Frostbite in case of prolonged direct exposure to the skin. Otherwise, it is an inert gas and humans have a very high tolerance to exposure. OSHA requirements effective 1 Mar 1990 specify a time weighted average (TWA) of 10,000 ppm and a short time exposure limit (STEL) of 30,000 ppm. This translates to a person being exposed to an average concentration of 10,000 ppm over an 8-hour workday, or a concentration of 30,000 ppm over 15 minutes (33).

### 3.4 Cost Concerns

Consideration should be given with regards to the costs associated with the deployment and operation of a seeding mechanism. The Sno-Gun II cleaning system for CO<sub>2</sub> has a retail price of approximately \$2,000.00, which is less than 20% the cost of conventional powder seeders. It should be noted that a commercial system for a large tunnel would likely be considerably more expensive.

The use of CO<sub>2</sub> for seed particles can provide additional cost savings when compared to other seed materials, as seen below (table 3.6) in the comparison between CO<sub>2</sub> and TiO<sub>2</sub>.

*Table 3.6: Cost comparison between TiO2 and CO2[8]*

Seed Material	Cost / lb	Density	Weight / Vol	Cost / m <sup>3</sup>
TiO2	\$7.72/ kg (3)	4230 k g / m3	4.22 x10 <sup>-3</sup> kg/m <sup>3</sup>	\$0.0325
Liquid CO2	\$0.44 / kg (4)	762 k g / m3	7.61x10 <sup>-4</sup> kg/m <sup>3</sup>	\$0.000335

TiO<sub>2</sub> is widely used as a seed material in gas flows, and while the cost savings of using CO<sub>2</sub> may not be applicable in smaller wind tunnels that require less seed material, larger scale facilities can expect to see considerable cost savings.

### 3.5 Considerations about CO<sub>2</sub>

In relation to our primary objective of choosing a particle material for all good reason mentioned above and explained later in the relevant sections, our attention was completely towards CO<sub>2</sub> as seed material. The good reasons for this were its good light scattering behaviour, small relaxation time, and above all very user friendly in terms of health and hazardous

effects. For this purpose we have to do some thermodynamical computations to see if CO<sub>2</sub> will work in our facility or not?

We had to use solid carbon dioxide (dry ice), and then this should be injected to the wind tunnel by using appropriate accessories. As this solid CO<sub>2</sub> will travel in the tunnel it will sublime directly to gaseous form. We had to calculate the time required for sublimation, so that we know that if solid CO<sub>2</sub> will reach our test section, in order for image processing. We utilized the equation below which is formed by using first law of thermodynamics. An energy balance between convective heat transfer and heat of sublimation will result.

$$(dp(t))^2 = (dp(i))^2 - \left[ \frac{4K_a Nu (T_\infty - T)}{\rho H v} \right] t \quad (3.9)$$

Here dp(t) is the particle diameter at some time. dp (i) is the initial particle diameter. Computations were made on the basis of above equation. Due to the high temperature of our facility, we found that CO<sub>2</sub> will not work. The life time of CO<sub>2</sub> was very short. Solid CO<sub>2</sub> was not able to reach the test section. Therefore, we left this option of using CO<sub>2</sub> as seed material and diverted our attention to Titanium Dioxide. The diameters of different CO<sub>2</sub> particles calculated with time are given in figure (3.5) below. The flow with steady state conditions reaches the test section between 3-5 ms. It is obvious from the figure plot that the life time of carbon dioxide is below the required time.

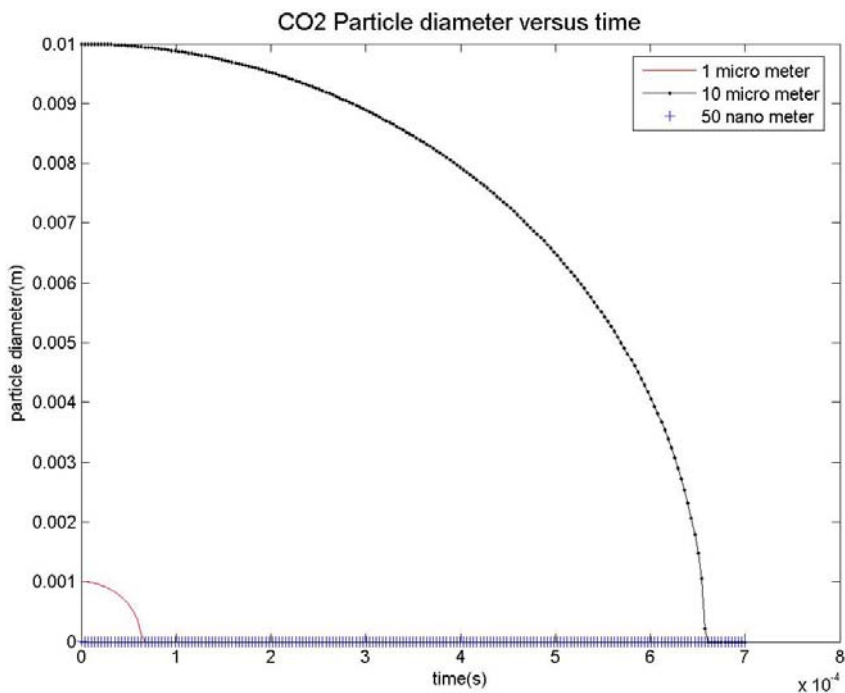


Figure 3.5. CO<sub>2</sub> Particle size with time

### 3.6 TiO<sub>2</sub> as Seed Material

Titanium dioxide is an appropriate seed material for all the good reasons discussed above. The small sized particles faithfully follow the flow and particle agglomeration is not a great problem in our facility. The only problem associated to the usage of Titanium dioxide is that it makes the facility very dirty, in turn it makes the windows dirty, causes the malfunctioning of the valves due to particles aggregation. We have chosen Titanium dioxide as a seed material because people in Technical University, Delft (Netherlands) successfully employed it and their flow conditions are very similar to ours.

Relaxation times of the particles of different sizes are calculated with Titanium dioxide ( $TiO_2$ ) density, 4230 kg/m<sup>3</sup>. The dynamic viscosity of air is 4.8297e-006 N.s/m<sup>2</sup>. The velocities of the particles of different sizes are shown in the figure (3.6). The scaled version of the figure is plotted as well.

It is obvious from the figure that the particles of sizes 21nm and 0.1 $\mu\text{m}$  attain the fluid velocity within no time, while the particles of larger size take some time to attain the fluid velocity. The relaxation times of the particles according to sizes are presented in the table (3.7).

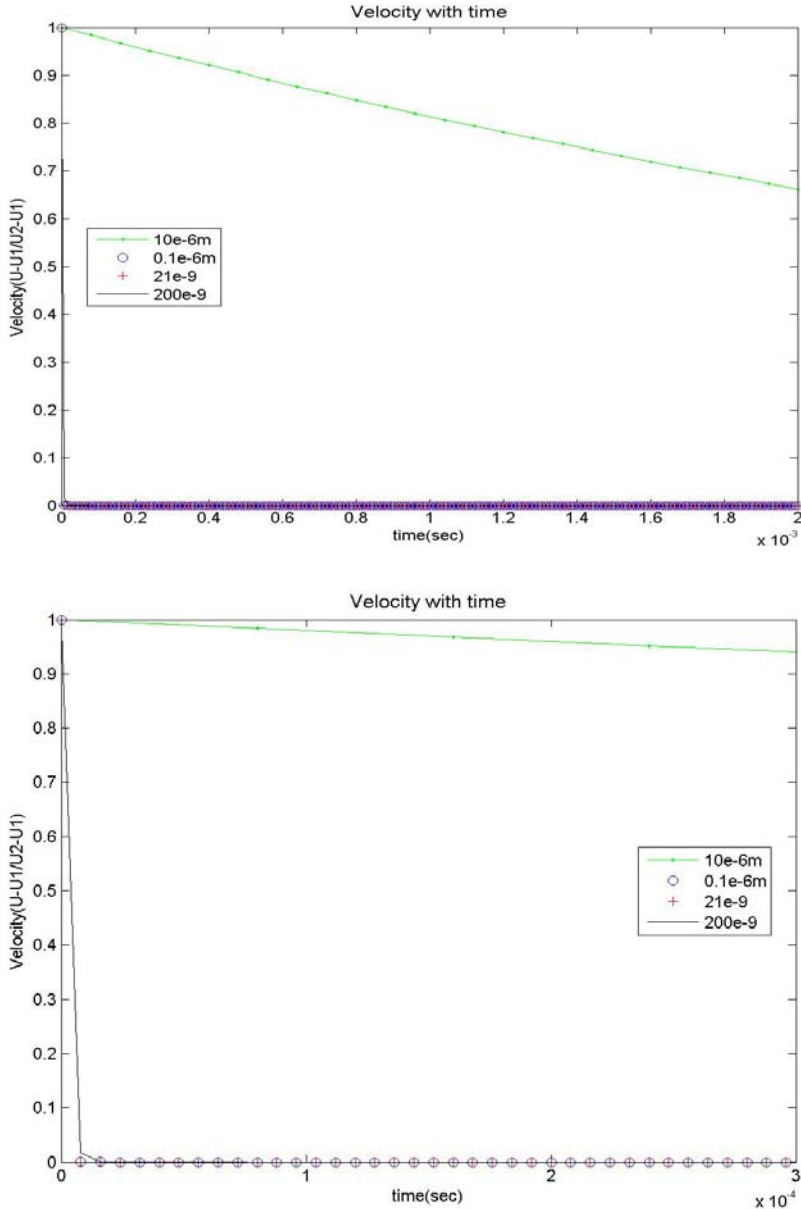


Figure 3.6. Particles velocity with time.

*Table 3.7. Titanium dioxide's particles relaxation time*

<b>Particle Diameter</b>	<b>Relaxation time</b>
0.021 $\mu\text{m}$	$2.14 \times 10^{-5}\text{ms}$
0.1 $\mu\text{m}$	$4.9 \times 10^{-4}\text{ms}$
0.2 $\mu\text{m}$	$1.9 \times 10^{-3}\text{ms}$
10 $\mu\text{m}$	4.9 ms

## 4 Seeding Generator and Seeding System

The next step after the conclusion of seeding material was to ponder about the way to inject the seeding particles into the facility in a way that the particles do not agglomerate too much and get distributed evenly in the tube. This arises the evolution of a seeding generator. The construction of the seeding generator is explained below.

The seeding generator consists of three parts. The main cylinder, top and the bottom lid. The top lid is having three holes in it. Through one side hole the particles are injected. Later in through experimentation it was discovered that the injection of particles through hole is not a suitable method, because in this way particles have to be pressed to pass through the funnel and pipe and particles do agglomerate in this way. Therefore to avoid this situation the particles are poured into the seeding generator through its mouth after removing the top lid. Therefore this hole was sealed. The other side hole is for the air inlet. Through this air inlet hole we inject a pipe of small diameter that is bent from the bottom at 45°. Also from experiments (explained below) it was found that this construction of pipe will not let many particles out of the seeding generator at low pressure ratios. This is because of the formation of particles clumps on the bottom of the seeding generator. Therefore a pipe with round bent at the bottom was chosen to serve the purpose effectively. The purpose of this pipe is to produce a cyclone inside the seeding generator so that the particles which are staying on the bottom are swirled and pushed upward. On the upper lid there is a hole in the centre. This hole is connected to the wind tunnel through pipe. Thus the particles travel through this hole and they pass to the wind tunnel just before the nozzle of the wind tunnel.

The design of the seeding generator involves some mechanics computations. The material of the seeding generator should possess the tensile strength to withstand the applied force. The material of the seeding generator is stainless steel. Also the required thickness of the cylinder is calculated. The lids are screw tightened to the main cylinder. Proper bolts were chosen and so were the holes drilled in the parts. The numbers of bolts required were also calculated. This is given in appendix A. The top and bottom lids were made air tight with the application of gaskets. Two

different seeding generators assemblies are shown in figure (4.1.a , 4.1.b). The reasons for these two different kinds of assemblies are explained later.

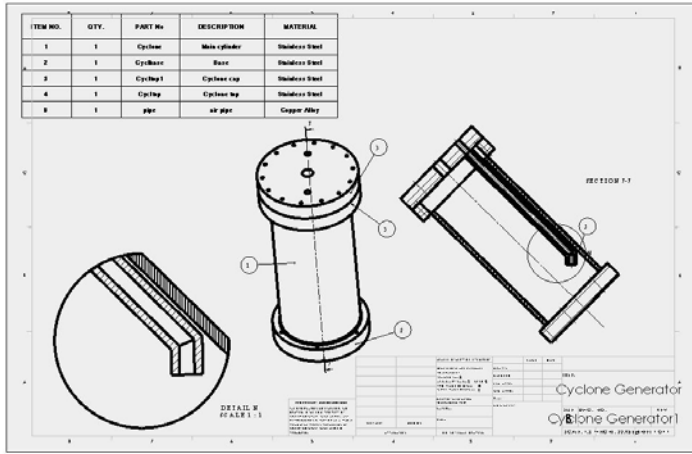


Figure 4.1.a. Seeding generator drawing with 45<sup>0</sup> bent air purging pipe.

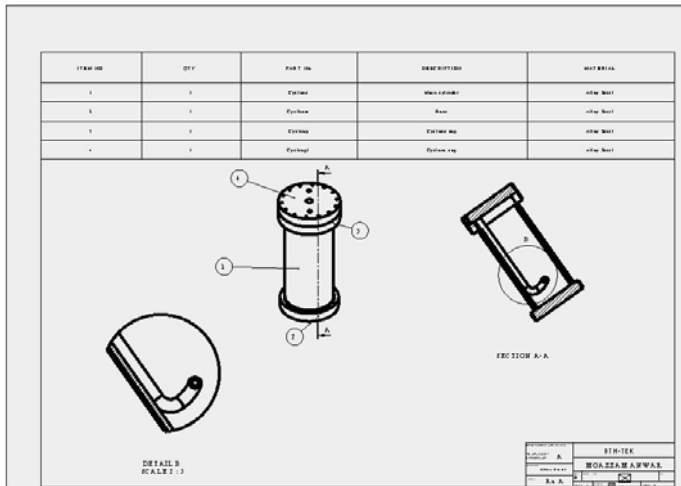


Figure 4.1.b. Seeding generator drawing with round bent air purging pipe.

The complete seeding system consists of several other accessories from the air transfer from the main high pressure (300bar) line (for the wind tunnel)

to the seeding generator, then for the transfer of seed particles to the tube. The following are the accessories needed for the whole seeding system.

1. Valves to control the flow of the air.
2. Pressure regulator to control the pressure.
3. Hose pipe and stainless steel pipes for the transfer of air.
4. Relief Valve.

A schematic diagram of the complete seeding system is shown below.

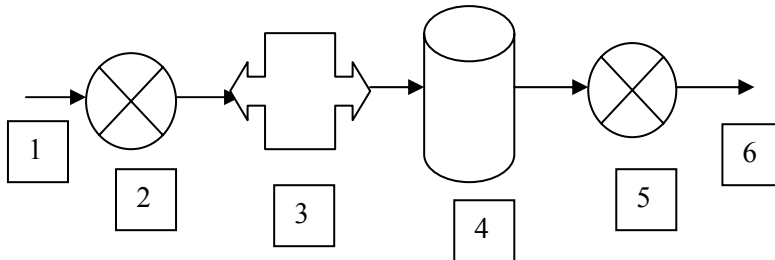


*Figure 4.2. Schematic sketch of seeding system*

The sequential blocks are narrating the following components.

1. High pressure (300bar) line.
2. Valve.
3. Pressure regulator.
4. Seeding Generator.
5. Valve.
6. Low pressure (10bar) line to Tube. This line is designed for 40 bar but we used 10 bar.

## **4.1 Experimentation with seeding system**

### **4.1.1 Particles Measurements**

The particles outcome from the seeding generator against different filling levels and pressure ratios between seeding generator and the pressure vessel was carried out to ensure that we have enough amounts of particles in the facility during experiments.

To continue in this regard, a pressure vessel was used. This pressure vessel allowed us to create a pressurized environment of desired level (1- 5 bars). The particles from the seeding generator were forced to accumulate in a polythene bag installed in the pressure vessel via the transfer line.

This was quite laborious work in a sense that first we need to install the polythene bag in the pressure vessel. Then the pressure vessel was pressurized and the seeding generator was pressurized to the desired point. The bag was removed after depressurizing the vessel to measure the particle outcome. This task was repeated several times. It was made sure that all the connections were same between the seeding generator and pressure vessel like those used in the real experiments.

The results of the experiments are tabulated and attached as appendix B. Some useful information regarding the amount of particles required for the experiments can be inferred from these tables. As a rule of thumb 10-25 particles are required for 1024 pixels area. Therefore, particles volume required for the experiments can be deduced from those tables.

Although the intricacies of the experiments as a whole cannot be explained for some unorthodox behaviour occurrence but still we can make some logical assumptions. These are categorized into two forms. One for the 45° degree bent air purging pipe and the second for the pipe bent round at the bottom.

For the 45° degree bent pipe the deductions are as follows,

1. At low pressure ratios, between seeding generator and Pressure vessel, also at low pressures great amount of particles sprang out of the seeding generator.
2. At high pressure ratios the amount of particles decreased.
3. For low pressure ratios, but at high pressures the amount of particles outburst also decreased.
4. As we went on increasing the pressure inside the pressure vessel, fewer amounts of particles was observed. This is due to the fact that pressure equalization obtained earlier.
5. The zero particle outcomes towards the end of the experiments can be rationalized by considering the fact that the particles had coagulated to a greater extent, which also blocked the air swirl.
6. For low seeding levels we can achieve great particles outcome.

7. In the end it is concluded that the 45° degree bent air purging pipe did not produce the proper swirl, rather it pushed the particles more to the walls.

Although we have not enough data for the air purging pipe bent round at the bottom, we have used this pipe successfully in real experiments.

This pipe produced proper swirl, which resulted in a great outburst of particles.

# 5 Experimental work

## 5.1 Facility Description

### 5.1.1 Working Principle

The Hypersonic Ludwig Tube Braunschweig(HLB) is designed for Mach number  $M=6$ . The operative range of the unit Reynolds number is between  $3 \cdot 10^6$  1/m and  $20 \cdot 10^6$  1/m. The test section has 500mm diameter and the time with near steady flow conditions is 80ms.

A schematic diagram of the HLB is given in Figure 5.1 [9].

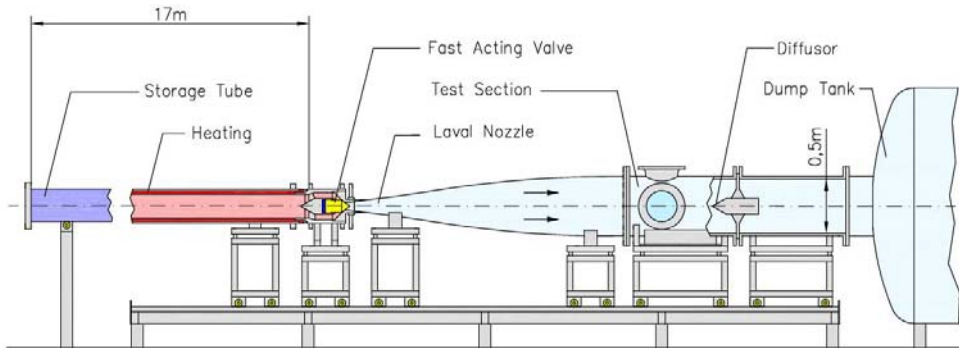


*Figure 5.1 Hypersonic Ludwig Tube Braunschweig(HLB)*

The assembly is divided into a high pressure and low pressure section, which are separated by the fast acting valve. The high pressure section consisting of the 17m long storage tube with a 3 m long heated section can be pressurized to up to 30 bar. The low pressure section consisting of the

hypersonic nozzle, the test section, the diffuser and a 6 m<sup>3</sup> dump tank is evacuated before each run to about 1mbar. The valve basically consists of a pneumatically driven piston which fits into the nozzle throat with its conical end. The valve can be opened for about 100ms. This causes an expansion wave to run into the storage tube. In the wave the air is accelerated towards the nozzle where it is expanded and accelerated to Mach 5.9 in the test section. The expansion wave travelling through the storage tube is reflected at its end and reaches the valve again after about 80 ms. This is the time period of the steady flow conditions in the test section. The closure of the valve inhibits complete equalization of pressure in the facility, which saves energy and time.

## 5.2 Hyperboloid Model

Flow investigations were carried out around an axisymmetric hyperboloid/flare model. The geometrical definition given by Schwane [10] resembles the contour of the windward side of the Hermes spacecraft at 30° angle of attack including a flap with 20% of the total length and a flap angle of 43.59° related to the axis or 22.28° related to the slope of the contour just before the hinge. The total length of the model is 149.24mm. The cylindrical portion has a length of 80mm. While the conical section and flap constitutes a length of 59.24mm. Figure 5.2 shows the geometry of the model with the shock topology at HLB conditions. Downstream of the bow shock, a recirculation zone develops along the hinge. The region of separated flow is bound by a separation and a reattachment shock. Downstream the flow is expanded across a Prandtl-Meyer expansion centred at the end of the flap. Models with different materials existed. The model we used is shown to the right and is made from PMMA.

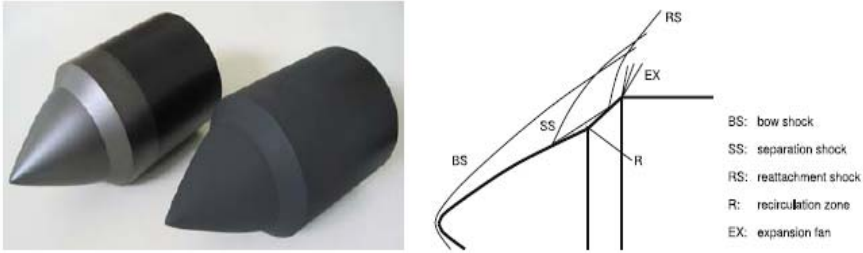


Figure 5.2. Hyperboloid/flare models; left model made from SINTIMID 15G, right model made from PMMA (left). Sketch of the shock topology around the model at an upstream Mach number of  $Ma=5.9$  (right)

### 5.3 Illumination and Photo acquisition system

The particles are illuminated by Double Pulsed Nd:YAG laser generating light pulses at a wavelength of 532nm with a maximum energy of 150mJ and a duration of 4.2ns. The laser light sheet thickness is 1mm, and the model is illuminated from the top.

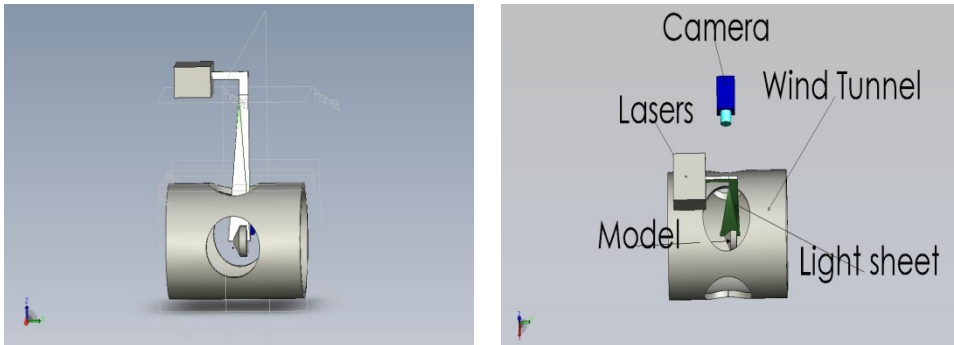


Figure 5.3. Schematic representation of PIV Setup

The light scattered by the particles is captured by a CCD camera in order to measure the spatial resolution. A PCO 4000 camera with  $4008 \times 2672 \text{ px}^2$  area was used to serve the purpose. The camera was placed perpendicular to the light sheet propagation axis. The distance between the PIV plane (light sheet) and the camera sensor was 0.90 m.

## 5.4 Experimentation

Before the commencement of real experiments, synchronization problems of the equipments were solved. It was made sure that the camera, laser and wind tunnel are perfectly synchronized, so that we capture the pictures of the flow within 80ms of the tunnel run time. The signals from camera running at 1.25 Hz were used to trigger the tunnel (vavle control). For this purpose *DaVis* software (developed by *LaVision*) and a sequencer card with phase shift (Hardsoft PTU 9) was used. In this respect trigger was set to recording rate. Also the settings for the valve control of the wind tunnel were accurately adjusted to create an offset. This offset was adjusted so that during the next trigger 800ms of camera, the flow was present. Accurate adjustment was necessary, because it was suspected that the seeding density would change during the tunnel run time. The repeatability of the triggering was assured by measuring signals from the fast acting valve and camera/laser. Five images were captured for one experiment. Image acquisition was set to trigger 3<sup>rd</sup> image.

Then the calibration was performed. The length (80mm) of the cylindrical portion was taken into account. This gave 2323 pixels for the length. Therefore the scale factor is,

$$M = \frac{80}{2323} = 0.0344mm/pix \quad (5.1)$$

Finally, the experiments were carried out. We could see the particles in the desired Image. Also particles movement was observed within the two frames of the Image. An example of one particle Image is shown in figure (5.1).

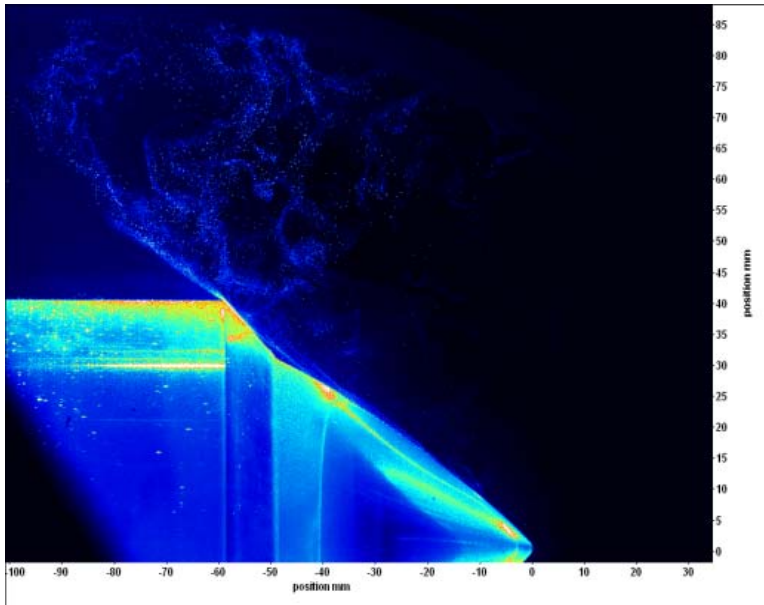


*Figure 5.4. PIV Image with Mach 5.9 around Hyperboloid flare configuration*

## 5.5 Data Processing

The cross-correlation of the PIV recordings is performed with DaVis. Two interrogation windows of sizes 250x250 and 60x60 pixels are used for the Data processing of the PIV with an overlap factor of 50 % each.

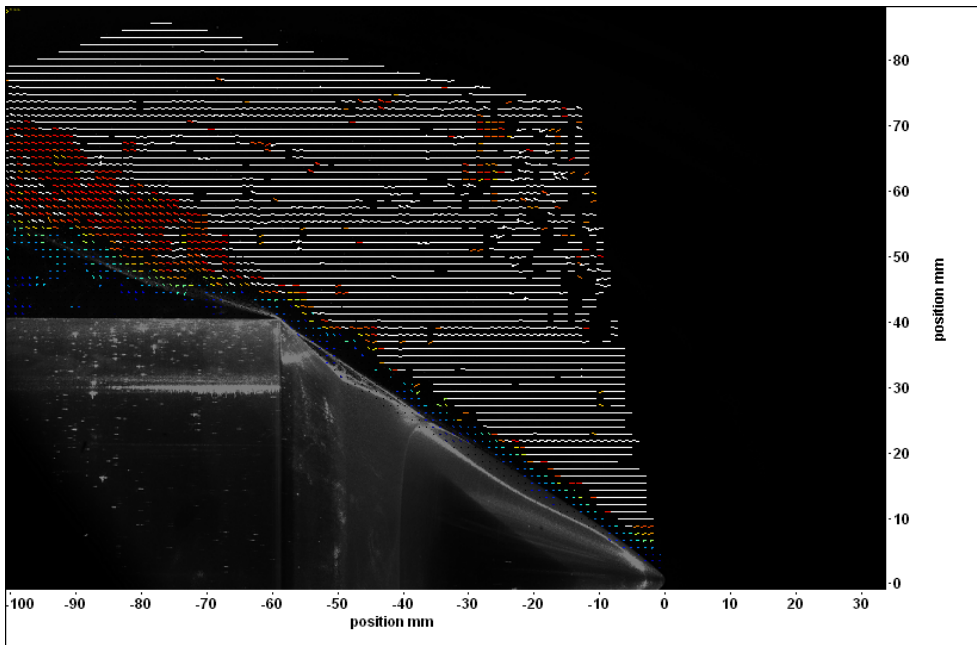


*Figure 5.5. Stream wise Velocity distribution*

The Image (5.5), shows the data processing results. The shocks were resolved with poor configuration. The data is Noisy because only one double frame was used. Usually several double frames are averaged. Here only one image could be recorded. This limitation is due the presence of particles in the test section at a specific time during the tunnel run time. The different colours in the Velocity distribution figure unfold the following information.

White= 941 m/s

Red = 740 m/s

Blue = 883 m/s

The repeatability of the experiments can be verified from the results of the different experiments. These are shown in the figures below.

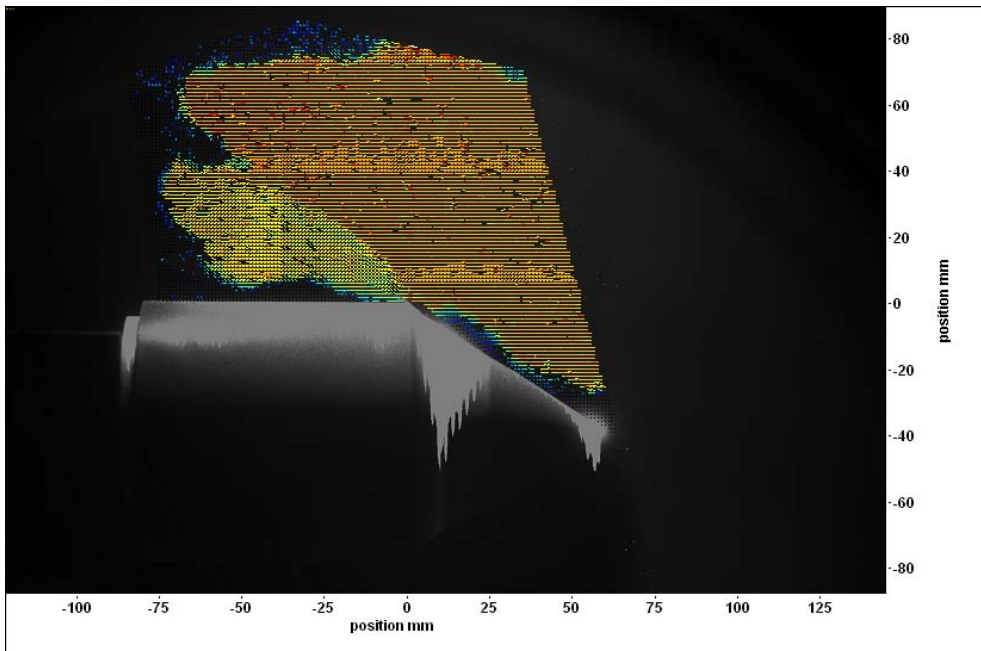


*Figure 5.6.a. PIV results from experiments*

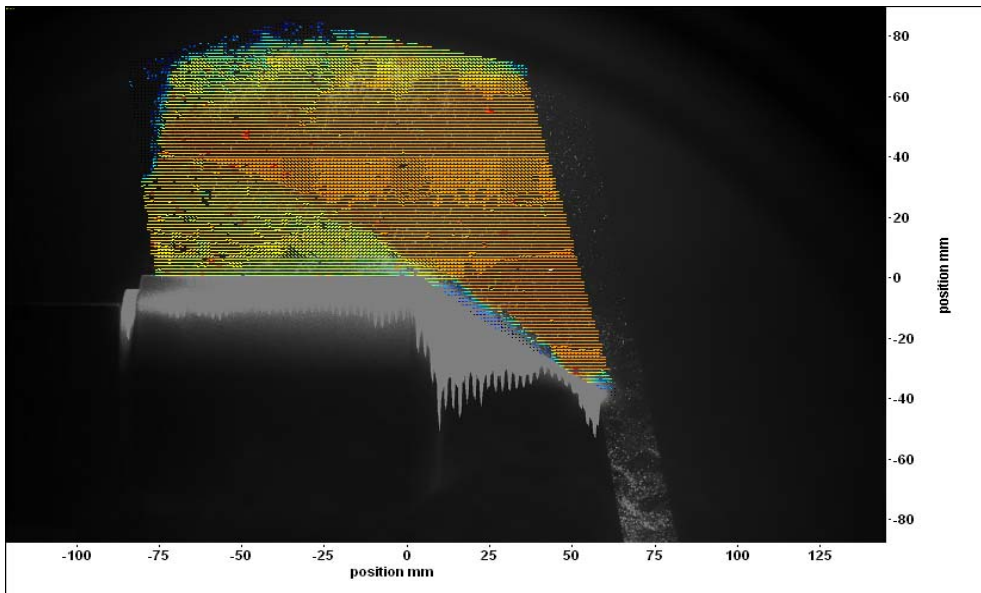


*Figure 5.6.b. PIV results from experiments*

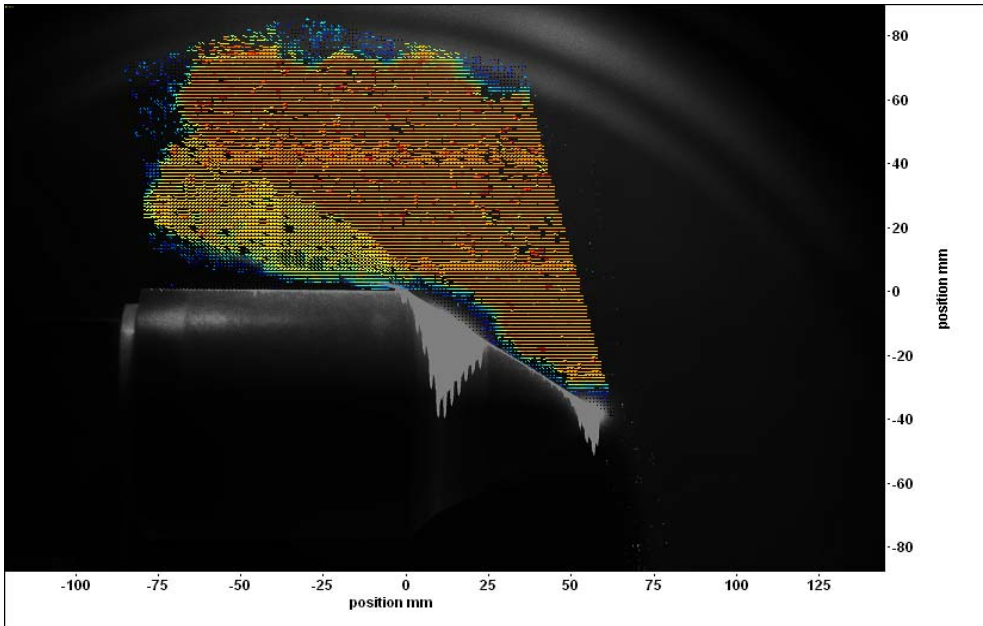


*Figure 5.6.c. PIV results from different experiments*

## **5.6 Comparison of Experimental work with Numerical Work**

A succinct summary of the comparison between different measuring techniques experimental and numerical work [11] is provided here. The figures (5.7.a, b, c and 5.8.a, b) are presented below for the comparison work. In these figures we have shown x-velocity as contour plot in the vicinity of the model.

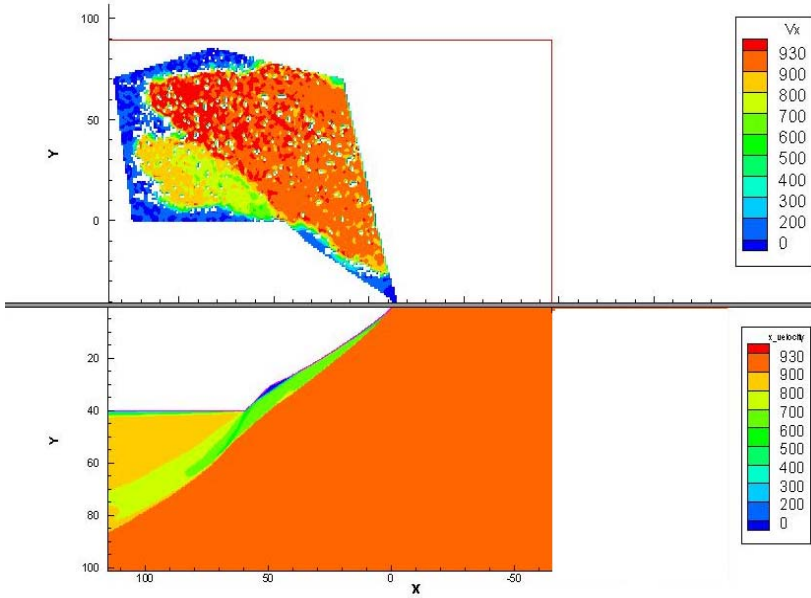


Figure 5.7.a. Comparison b/w experimental work(above) and numerical work(below).

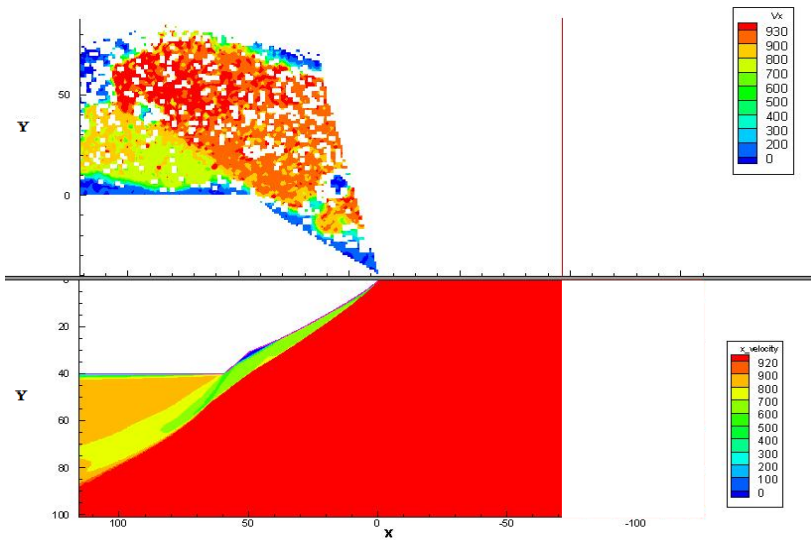
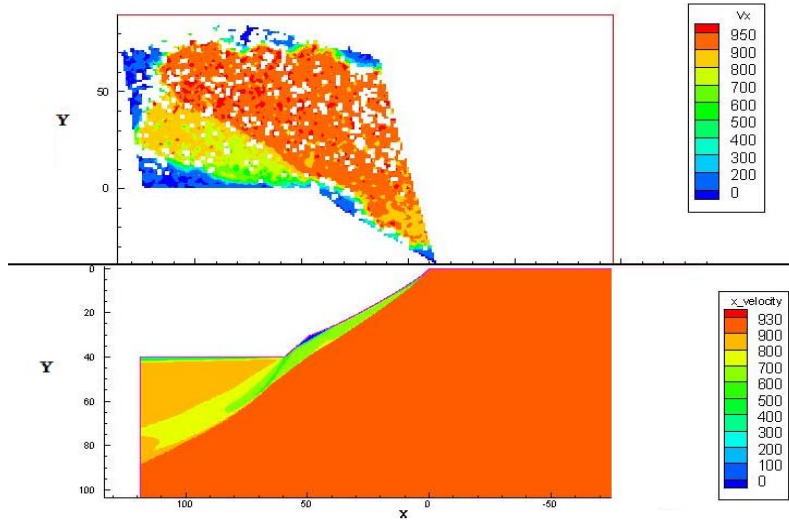


Figure 5.7.b. Comparison b/w experimental work(above) and numerical work(below).



*Figure 5.7.c. Comparison b/w experimental work(above) and numerical work(below).*

The pictures from different experiments with their corresponding comparisons with numerical work (computed with TAU code) [11] are shown above. All comparison figures show experimental results above and numerical work below. We can clearly see the similarities between experimental and numerical work. All the figures above show similar behaviour with very small differences. The differences are present due to the varying particle density. This particle variation is a result of seeding generator filling level. Like in the very first figure at the nose we see a little glitch. This is due the loss of particles. But we can appreciate the great similarities between the figures as a whole.

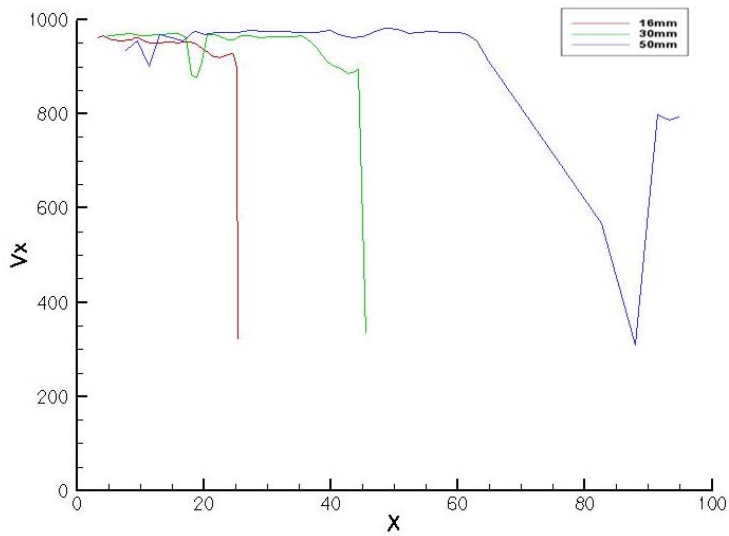


Figure 5.8.a. Plot of velocities at different heights along the model, experimental (above), numerical (below).

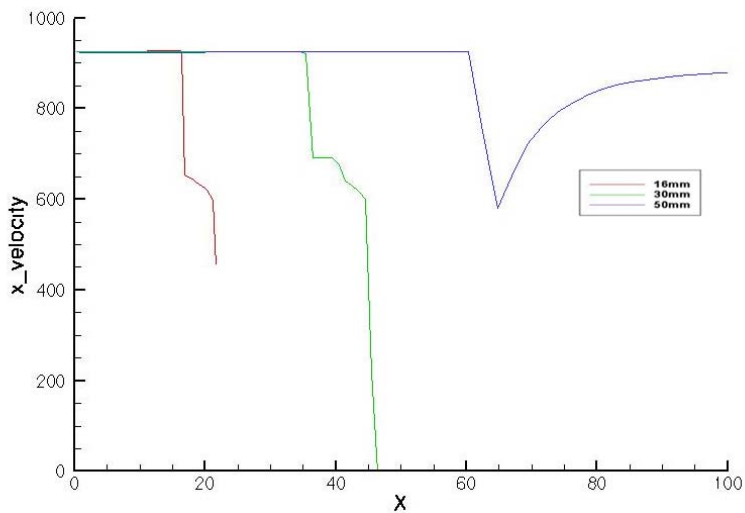


Figure 5.8.b. Plot of velocities at different heights along the model, experimental (above), numerical (below).

Figures (5.7.a, b, c) can be understood well while referring to the figure (5.2). The experimental results (above) and numerical results (below) are very much in accordance with each other with small discrepancies. The positions of the shocks are alike. The presence of bias error (in magnitudes of velocities) can be upto 20% within experimental results which is assumed on the basis of studies made by (G.E. Elsinga, B.E. van Oudheusden, F, Scarano) [12] are due to the gradient of the optical displacement vector ( $\nabla\xi$ ). This contributes to the direct velocity error.

The blue nebula present across the model in figure (5.7.a, b, and c) is due to the loss of particles.

The plots of the velocities at different heights along the model also show some deviations. The velocities are taken along constant lines at certain heights. The shapes of the plots are more or less same. The higher velocities at ( $x=18-20\text{mm}$ ,  $y=16\text{mm}$ ) and at ( $x=38-42\text{mm}$ ,  $y=30\text{mm}$ ) in experimental results are due to inertial waves of the particles. At ( $x=60-84\text{mm}$ ,  $y=50\text{mm}$ ), the steep decline in the velocities can be attributed to the loss of particles.

## 5.7 Image Position Error

The inhomogeneous nature of the fluid as in case of compressible flows or thermal convection flows can cause a local distortion of the image of the illuminated particles in the process of image acquisition. The image pattern of the particles resulting from such experiments is then subjected to deformation and individual particles may be perceived as blurred. In the case of particle image velocimetry two kinds of errors can be identified: position error and velocity error.

These position and velocity errors result from the geometrical deformation of the image, which cause a systematic (bias) error of the measured velocity. In synthesis one may say that the wrong velocity vector is evaluated at the wrong position. Image blur affects the tracking precision in terms of cross-correlation accuracy due to the (anisotropic) increase of the particle image size, thus broadening the correlation peak. This is illustrated with the help of figure (5.8) [12].

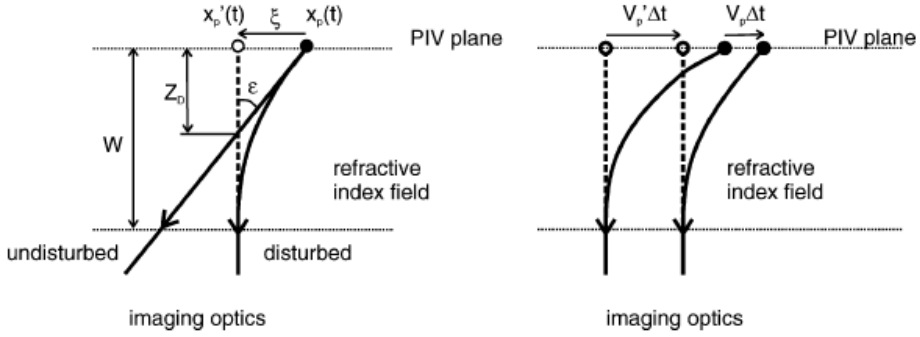


Figure 5.8. Optical distortion in PIV: position error (left) and direct velocity error (right). Solid lines represent light ray trajectories coming from the particle (solid circle). Dashed lines are backward extension of those rays indicating the position where the particle is perceived in the PIV plane (open circles)

Let the image distortion be expressed in terms of an optical displacement vector  $\vec{\xi}(\vec{x})$ , as:

$$\vec{\xi}(\vec{x}_p(t)) = \vec{x}_p'(t) - \vec{x}_p(t) \quad (5.3)$$

Where  $\vec{x}_p(t)$  is the actual particle location (x , y) in the measurement plane and  $\vec{x}_p'(t)$  is the location where that particle is perceived (Figure 5.8, left). The optical displacement vector is directly equivalent to the position error of the measurement and is related to the gradient of the refractive index  $\nabla n$ . The Backward Oriented Shlieren technique (BOS) studies (Richard and Raffel 2001[13]; Elsinga et al 2004a[14]) propose the following expression for the optical displacement vector based on the theory of light propagation in a refractive index field (using  $n \sim 1$ ) :

$$\vec{\xi}(\vec{x}) = -Z_D \vec{\epsilon}(\vec{x}) = -Z_D \int_S \nabla n(\vec{x}, z) dz \quad (5.4)$$

Where z is the coordinate direction normal to the PIV measurement plane,  $\epsilon$  the light beam deflection angle and  $Z_D$  is the distance parallel to the

optical axis between the measurement plane and the intersection point of the disturbed ( $\nabla n \neq 0$ ) and the undisturbed ( $\nabla n = 0$ ) light rays coming from the same particle (Fig. 1 left). The refractive index  $n$  depends on the density  $\rho$  according to the Gladstone-Dale relation, i.e.

$$n = 1 + K\rho \tag{5.5}$$

Where  $K = 2.3 \times 10^{-4} \text{ m}^3/\text{kg}$  for air.

Equation (5.4) was used to compute the particle position error at different coordinates ( $x, y$ ) along the model. To compute the value of  $n$  the values the densities  $\rho$  were taken from the numerical work [11] along those coordinates. Matlab codes were generated to approximate the data as well as to compute the position error. 10<sup>th</sup> degree polynomials were found to be good approximations. The approximated polynomial was used to find the refractive index gradient by using Matlab command (`diff(n,z)`), then the integration of the above equation (5.4) was done using Matlab command (`quad`). One figure of the data approximation with the 10<sup>th</sup> degree polynomial is shown (5.9).

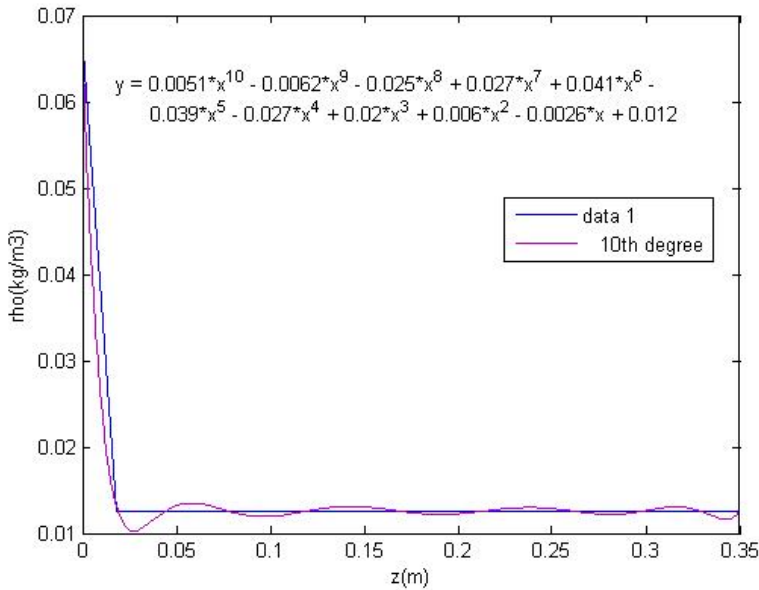


Figure 5.9. 10<sup>th</sup> degree polynomial fit to the data

The computed error values are mentioned below with their corresponding positions.

$\xi(\vec{x}) = 0.1168 \mu\text{m}$  at (0, 0) at the start of the bow shock.

$\xi(\vec{x}) = 0.0011 \mu\text{m}$  at (40, 60) in the free stream zone above the bow shock.

$\xi(\vec{x}) = 7.3287 \times 10^{-5} \mu\text{m}$  at (62, 52) just before the reattachment shock.

$\xi(\vec{x}) = -0.0088 \mu\text{m}$  at (67, 52) inside the reattachment shock.

$\xi(\vec{x}) = -0.0879 \mu\text{m}$  at (75, 52) further inside the reattachment shock.

$\xi(\vec{x}) = -0.0667 \mu\text{m}$  at (100, 52) far inside the reattachment shock.

For the coordinates of these points refer to the figure below (5.10)

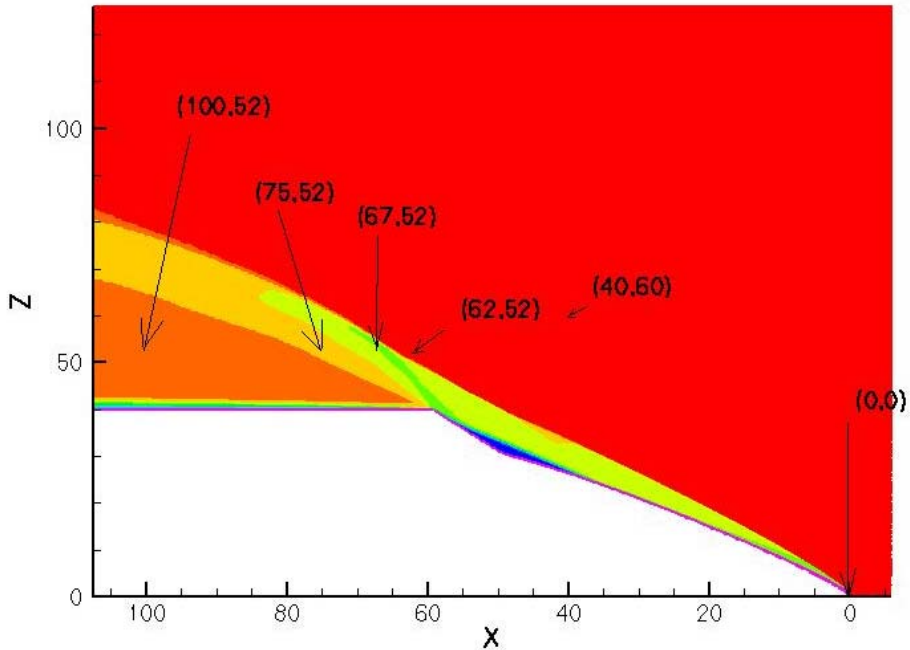


*Figure 5.10. Coordinates location of the points where image position errors were calculated*

## 6 Conclusions

Particle Image Velocimetry (PIV) setup was installed for the application in hypersonic flows with Mach no (5.9) around a hyperboloid flare configuration.

Some considerations for the seeding materials were taken into account. This include the scattering characteristics, tracking behaviour of the particles, Health and Hazardous impacts and cost concerns. CO<sub>2</sub> was found most appropriate as seeding material. But thermodynamical calculation proved that CO<sub>2</sub> cannot be used for our experiments. This is because of the high temperatures of our facility. The life time of CO<sub>2</sub> was very short. Like for 10 micro meter particle it is 0.65 ms. While the flow under steady state conditions reaches the test section between 3-5 ms from the fast acting valve of the Hypersonic Ludwig tube. Then Titanium dioxide was considered as seed material. Titanium dioxide TiO<sub>2</sub> was selected as seeding material. A relaxation time of  $1.9 \times 10^{-3}$  ms was calculated for the 0.2  $\mu\text{m}$  particle size, because on the basis of available information particles of this size were expected after agglomeration.

Seeding generator was designed for the homogeneous distribution of the particles into the wind tunnel. Proper design considerations were taken so that the seeding generator can sustain pressure upto 50 bars. This include the selection of proper material like stainless steel, calculations for the effective thickness of the wall of the seeding generator and the proper selection of the no and type of the bolts.

Pressure test was performed on seeding generator to ensure the safe handling of seeding generator.

Prior to the commencement of real experiments synchronization issues of the equipment were resolved. It was made sure that the laser running at frequency (10Hz), and camera with frequency (1.25Hz) are perfectly synchronized with the tunnel run time of 80ms. Further to this end, an offset in the valve timing of the tunnel was created to make it sure that the laser and camera triggering occurs when the flow is present in the test section. The repeatability of the experiments was also ensured by measuring the signals from fast acting valve and laser/camera.

Shock waves were resolved, corresponding to the available Schliern and numerical results. Although the shocks are not as good resolved as in the

numerical work, but the results can be very well appreciated for the presence of bow shock and reattachment shock. The velocities across the shocks and free stream regions and the deflections of the flow are in accordance with the numerical work with some bias error.

Particle position error was calculated. In this regard the equation derived by (Richard and Raffel 2001[13]; Elsinga et al 2004a[14]) was used. The density values to be used in this equation to find refractive index gradient were taken from numerical work (TAU calculations) [11]. A Matlab code was generated to compute the values. The calculated error values were found very small due to the low density of the flow.

## **7 Recommendations for Future Research**

The current research work presents a successful application of planar (2D) PIV in hypersonic flows. 3D PIV should be applied to hypersonic flows to measure instantaneous 3D velocity fields. Of the already available 3D PIV techniques (Holographic PIV, Scanning PIV and 3D Particle tracking Velocimetry), Holographic PIV and 3D Particle tracking Velocimetry can be applied to the hypersonic flows.

Holographic PIV(Hinsch 2002[15], Chan et al 2004[16], Arroyo and Hinsch 2007[17]) is most fascinating technique. In this technique the light scattered by the particles is made to interfere with the reference light beam. The interference effect is then recorded locally onto the holographic plate. Several millions of velocity vectors can be extracted from a good quality hologram.

The problems of magnification and poor image contrast in the holographic records can be eliminated by having the playback beam of the same wavelength and wave front characteristics as the recording reference beam.

## 8 References

1. M.Raffel,C.E.Willert,J.Kompenhans (2000): Particle Image Velocimetry.
2. J.Westerweel, Meas.Sci.Tech.8,1997.
3. A.Melling(1997), Tracer Particles and seeding materials for particle image velocimetry.
4. Durst F, Melling A and Whitelaw J H 1981 *Principles and Practice of Laser-Doppler Anemometry* (London: Academic).
5. A.B. Basset, Treatise on hydrodynamics, vol. 2 (original publication 1888), Deighton, Bell and Co., Cambridge, 1961.
6. Raffel, M. Willert, C. Kompenhans J (1998): Particle Image Velocimetry, A Practical Guide .
7. Samimy, M., Lele, S.K. (1991): Motion of particles with inertia in a compressible free shear layer. *Physics of Fluids*.
8. Charles J. DeLapp, II, BS Major: USAF (2006), Particle image velocimetry using novel, non-intrusive particle seeding.
9. M. Estorf, T.Wolf, and R.Radespiel: Experimental and numerical investigations on the operation of the Hypersonic Ludwig Tube Braunschweig. 5th European Symposium on Aerothermodynamics for Space Vehicles, 2004.
10. Schwane, R.: Description of the testcase: MSTP workshop 1996 reentry aerodynamics and ground-to-flight extrapolation. Technical Report YPA/1889/RS, ESTEC, Noordwijk (1996).
11. T.Wolf. M.Estrof. R.Radespiel ,(2007), Investigation of the starting process in a Ludwig tube .
12. G.E. Elsinga, B.W. van Oudheusden, F.Scarano (2005), Evaluation of aero-optical distortion effects in PIV.
13. Richard H, Raffel M (2001) Principle and applications of the background oriented schlieren (BOS) method. *Meas Sci Technol* 12:1576–1585.

14. Elsinga GE, van Oudheusden BW, Scarano F, Watt DW (2004a) Assessment and application of quantitative schlieren methods: calibrated color schlieren and background oriented schlieren. *Exp Fluids* 36:309–325.
15. Hinsch KD (2002) Holographic particle image velocimetry. *Meas Sci Technol*, Vol 13, R61-R72
16. Chan VSS; Koek WD; Barnhart DH; Bhattacharya N; Braat JJM; Westerweel J (2004) Application of holography to fluid flow measurements using bacteriorhodopsin (bR). *Meas Sci Technol*, Vol 15, 647-655
17. Arroyo MP; Hinsch KD (2007) Recent developments of PIV towards 3D measurements. In: *Particle image velocimetry: New developments and recent applications*. Ed. Schröder A; Willert CE, Springer, Berlin Heidelberg New York

# Appendix A

Bolt Selection Formula

$$\Delta P * A = \frac{\sigma_{max}}{S.A_{bolt}} * n_{bolt}$$

Where,

$\Delta P$  = total pressure on the surface (top lid),

$A$  = Area of the surface (top lid),

$\sigma_{max}$  = tensile strength of bolt,

$S$  = Safety factor,

$A_{bolt}$  = Area of the bolt,

$n_{bolt}$  = no of bolts.

# Appendix B

## Particle Measurements

### Experiment no 1

Seeding generator was filled with a particles volume 170 ml through the air inlet port. The air was purged into the seeding generator through a pipe bent at 45° at the bottom.

### Observations

S.G=Seeding Generator

P.V=Pressure Vessel

S.G Pressure(bar)	P.V Pressure(bar)	Particle Volume(ml)	Seeding Level(ml)
2	1	5	170
3	1	5	165
4	1	0	165
5	1	0	165
6	1	0	165
7	1	0	165
8	1	0	165

Seeding generator was opened and it was observed that great amount of particles stick to the wall and also particles coagulated at the bottom.

# Particle Measurements

## Experiment no 2

Seeding generator was filled with a particles volume 200 ml through its mouth after removing the top lid. The air was purged into the seeding generator through a pipe bent at 45° at the bottom.

## Observations

S.G=Seeding Generator

P.V=Pressure Vessel

S.G Pressure(bar)	P.V Pressure(bar)	Particles Volume(ml)	Seeding Level(ml)
2	1	70	200
3	1	35	130
2	1	50	95

Seeding generator was opened and a clump of particles as well as powdered particles were observed.

# Particle Measurements

## Experiment no 3

Seeding generator was filled with a particles volume 400 ml through its mouth after removing the top lid. The air was purged into the seeding generator through a pipe bent at 45° at the bottom.

## Observations

S.G=Seeding Generator

P.V=Pressure Vessel

S.G Pressure(bar)	P.V Pressure(bar)	Particles Volume(ml)	Seeding Level(ml)
2	1	50	400
3	1	42	350
2	1	55	308
3	1	42	253
4	1	40	211
5	1	0	211

Seeding generator was opened and clumps of particles as well as powdered particles were observed.

# Particle Measurements

## Experiment no 4

Seeding generator was filled with a particles volume 400 ml through its mouth after removing the top lid. The air was purged into the seeding generator through a pipe bent at 45° at the bottom.

## Observations

S.G=Seeding Generator

P.V=Pressure Vessel

S.G Pressure(bar)	P.V Pressure(bar)	Particles Volume(ml)	Seeding Level(ml)
4	1	14	400
5	1	14	386
4	1	50	372
5	1	14	322
4	1	32	308
5	1	20	276
4	1	20	256
5	1	14	242
4	1	0	242
6	1	0	242

Seeding generator was opened and clumps of particles as well as powdered particles were observed.

# Particle Measurements

## Experiment no 5

Seeding generator was filled with a particles volume 400 ml through its mouth after removing the top lid. The air was purged into the seeding generator through a pipe bent at 45° at the bottom.

## Observations

S.G=Seeding Generator

P.V=Pressure Vessel

S.G Pressure(bar)	P.V Pressure(bar)	Particles Volume(ml)	Seeding Level(ml)
6	1	20	400
7	1	8	380
8	1	20	372
6	1	15	352
7	1	8	337
8	1	0	337

Seeding generator was opened and clumps of particles as well as powdered particles were observed.

# Particle Measurements

## Experiment no 6

Seeding generator was filled with a particles volume 400 ml through its mouth after removing the top lid. The air was purged into the seeding generator through a pipe bent at 45° at the bottom.

## Observations

S.G=Seeding Generator

P.V=Pressure Vessel

S.G Pressure(bar)	P.V Pressure(bar)	Particles Volume(ml)	Seeding Level(ml)
3	2	0	400
4	2	2	400
5	2	1	398
3	2	8	397
4	2	8	389
5	2	6	383

Seeding generator was opened and clumps of particles as well as powdered particles were observed.

# Particle Measurements

## Experiment no 7

Seeding generator was filled with a particles volume 400 ml through its mouth after removing the top lid. The air was purged into the seeding generator through a pipe bent at 45° at the bottom.

## Observations

S.G=Seeding Generator

P.V=Pressure Vessel

S.G Pressure(bar)	P.V Pressure(bar)	Particles Volume(ml)	Seeding Level(ml)
6	2	2	400
7	2	2	398
8	2	5	396
6	2	0	391
7	2	0	391
8	2	0	391

Seeding generator was opened and clumps of particles as well as powdered particles were observed.

# Particle Measurements

## Experiment no 8

Seeding generator was filled with a particles volume 400 ml through its mouth after removing the top lid. The air was purged into the seeding generator through a pipe bent at 45° at the bottom.

## Observations

S.G=Seeding Generator

P.V=Pressure Vessel

S.G Pressure(bar)	P.V Pressure(bar)	Particles Volume(ml)	Seeding Level(ml)
6	5	1.8	400
7	5	0	398.2
8	5	0	398.2
9	5	0	398.2
10	5	0	398.2

Seeding generator was opened and clumps of particles as well as powdered particles were observed.

# Particle Measurements

## Experiment no 9

Seeding generator was filled with a particles volume 210 ml through its mouth after removing the top lid. The air was purged into the seeding generator through a pipe bent at 45° at the bottom.

## Observations

S.G=Seeding Generator

P.V=Pressure Vessel

S.G Pressure(bar)	P.V Pressure(bar)	Particles Volume(ml)	Seeding Level(ml)
10	5	14	210
10	5	3	196
10	5	12	193
10	5	7	181

Seeding generator was opened and clumps of particles as well as powdered particles were observed.

# Particle Measurements

## Experiment no 10

Seeding generator was filled with a particles volume 250 ml through its mouth after removing the top lid. The air was purged into the seeding generator through a pipe bent at 45° at the bottom.

## Observations

S.G=Seeding Generator

P.V=Pressure Vessel

S.G Pressure(bar)	P.V Pressure(bar)	Particles Volume(ml)	Seeding Level(ml)
7	5	16	234
8	5	0	218
8	5	0	218
9	5	0	218
10	5	0	2

Seeding generator was opened and clumps of particles as well as powdered particles were observed.

# Particle Measurements

## Experiment no 11

Seeding generator was filled with a particles volume 250 ml through its mouth after removing the top lid. The air was purged into the seeding generator with a pipe bent round at the bottom.

## Observations

S.G=Seeding Generator

P.V=Pressure Vessel

S.G Pressure(bar)	P.V Pressure(bar)	Particles Volume(ml)	Seeding Level(ml)
10	5	50	250
10	5	50	5





---

Department of Mechanical Engineering, Master's Degree Programme  
Blekinge Institute of Technology, Campus Gräsvik  
SE-371 79 Karlskrona, SWEDEN

Telephone: +46 455-38 55 10  
Fax: +46 455-38 55 07  
E-mail: [ansel.berghuvud@bth.se](mailto:ansel.berghuvud@bth.se)